

1 Final Report of the  $\bar{P}$ ANDA PID TAG

2 Draft 0.2

G. Schepers, GSI Darmstadt, et al.

3	<b>Contents</b>	
4	<b>1 Introduction</b>	<b>3</b>
5	<b>2 Physics Requirements</b>	<b>4</b>
6	<b>3 Tools</b>	<b>5</b>
7	3.1 Separation Power . . . . .	6
8	3.2 Phase space plots . . . . .	7
9	3.3 Fast Simulation . . . . .	8
10	<b>4 PID Subsystems</b>	<b>9</b>
11	4.1 Central Tracker . . . . .	10
12	4.1.1 Time Projection Chamber (TPC) . . . . .	11
13	4.1.2 Straw Tube Tracker (STT) . . . . .	13
14	4.2 Time of Flight (ToF) . . . . .	14
15	4.3 Barrel DIRC . . . . .	15
16	4.4 Barrel Calorimeter . . . . .	16
17	4.5 Forward Cherenkov . . . . .	17
18	4.5.1 Focussing Disc DIRC . . . . .	18
19	4.5.2 Time of Propagation Disc DIRC . . . . .	20
20	4.5.3 Proximity RICH . . . . .	21
21	4.5.4 Forward RICH . . . . .	22
22	4.6 Forward Calorimeter . . . . .	23
23	4.7 Muon Counter . . . . .	24
24	<b>5 Evaluation</b>	<b>25</b>
25	5.1 Potential of the Subsystems . . . . .	25
26	5.2 Matching of the Subsystems . . . . .	25
27	<b>6 Global PID Scheme</b>	<b>26</b>
28	<b>7 Conclusion</b>	<b>27</b>
29	<b>8 Acknowledgments</b>	<b>28</b>
30	<b>9 Appendix</b>	<b>30</b>

# 1 Introduction

The PANDA ([1]) PID TAG (Particle Identification Technical Assessment Group) was installed to give to the collaboration a complete set of parameters for an optimal set of particle detectors. The task given to this TAG is described in more detail:

## Subject

- Requirements from physics
- Evaluate potential of each subsystem
- Matching of systems

## Deliverables

- Definition of global PID scheme
- Optimized set of detectors and parameters

This list reflects roughly the structure of the PID TAG work and of this report. In an additional subsection the tools available for the PID TAG work are presented and explained (see also [2]) . The PID TAG evaluated the necessity of mapping the "Separation Power" in dependence of the momentum and the polar angle of the reaction products which is described in section 3.1. Since a "full simulation" was not available to calculate the performance of all the sub detectors, the TAG gathered parameterizations of the single sub detectors which went into a "Fast Simulation" explained in section 3.3. For single physics channels a "Full Simulation" was used.

Amongst others some important questions to solve were:

- PID with and with out the information of a Time Projection Chamber (TPC)
- PID with and with out an Forward Endcap Cherenkov, and with different forms (Focusing Disc DIRC, Time of Propagation Disc DIRC and Proximity RICH)
- PID with and with out a Forward RICH

The PID TAG had about 10 presence meetings and over 15 on line meetings. First PID subsystems were defined. Each subsystem has its responsible representative. Each representative had a replacement of his own group to guarantee always the same level of knowledge in all subsystems. For special subjects experts were asked to present informations in the meeting or to give answers to questions which arose.

The members of the TAG and their special responsibilities are listed at the end of the document (section 9).

## 2 Physics Requirements

The HESR (High Energy Storage Ring) of the new FAIR (Facility for Antiproton and Ion Research) project provides an Antiproton beam of high resolution (down to  $\Delta p = 1 \times 10^{-5}$ ) and intensity from 1.5 GeV/ $c$  to 15 GeV/ $c$  momentum.

This offers the unique possibility of investigating a broad field of physics. The vast variety of reaction types from meson-production over Charmonium decays to Hyper nuclear reactions demands a complete and compact detector system.

The physics requirements to the detectors are:

- to cover the full angular range of the physics products
- to detect all momenta of the reaction products
- to separate particle types with a defined level of separation over the full range of momenta of the reaction products.

The full solid angle can only be covered by the full set of detectors. Sometimes the momentum coverage has to be fulfilled by a combination of two or even three sub detectors.

For the single subsystems benchmark-channels had to be identified (Table 1) and simulated.

Channel	Final state	Related to detector
$\bar{p}p \rightarrow (n)\pi^+\pi^-$	$(n)\pi^+\pi^-$	EMC
$\bar{p}p \rightarrow \psi(3770) \rightarrow D^+D^-$	$2K 4\pi$	DIRCs, ToF
$\bar{p}p \rightarrow \eta_c \rightarrow \phi\phi$	4K	DIRCs
$\bar{p}p \rightarrow D_S D_{S0}^*(2317)$	$\pi^\pm K^+ K^-$	DIRCs
		muon
		Forward RICH

Table 1: Benchmark channels to evaluate the performance of the different PID detectors.

At  $\bar{P}$ ANDA  $2 \times 10^7$  reactions per second with up to 10 charged particles per reaction have to be digested by the detectors.

## 79 **3 Tools**

80 In this section the TAG work is described. To evaluate the performance of the detectors the PID  
81 TAG defined the "Separation Power" as the right tool (see section 3.1. With the help "Phase  
82 Space Plots" (section 3.2) the angular coverage and the corresponding particle momenta could be  
83 determined. The "Fast Simulation" (section 3.3) was used to map the separation power over  
84 the full angular and momentum range. In a second step important reactions and their relevant  
85 background channels were simulated. Thus the regions where a good separation power is needed  
86 could be identified and checked whether the detector performance is sufficient there.

### 3.1 Separation Power

The PID TAG decided to use the separation power with the sigma separation value defined as

$$\sigma_{sep} = \frac{|m_A - m_B|}{\sigma_B} = \frac{|m_A - m_B|}{(\sigma_A/2 + \sigma_B/2)}$$

where A and B are two different particle types of the same momentum. The masses  $m_A$ , respectively,  $m_B$  are Gauss distributed with the  $\sigma$  being the standard deviation.

The particle flux (so different amplitudes of the distributions) was not taken into account as well as different width or even shapes of the distributions. Nevertheless this definition can give a qualitative measure to the detector performance needed for their evaluation. In the calculation with the Fast Simulation the definition of the separationpower, however, varied slightly, allowing different widths of the Gaussian distributions of both particles (3.3).

## <sup>96</sup> 3.2 Phase space plots

<sup>97</sup> Following a request of the PID TAG phase space plots from all the reactions relevant for the  
<sup>98</sup> physics book were produced. The set of plots shows for each particle species of the reaction the  
<sup>99</sup> particle momentum versus theta angle and the transversal versus the longitudinal momentum.

### 100 **3.3 Fast Simulation**

101 In order to get information about phase space (.i.e. momentum-theta dependence) coverage of  
102 the different PID relevant subsystems maps of separation power have been generated based on  
103 fast simulations of single track events, i.e. the particles properties are modified with an effective  
104 parametrization of detectors responses and PID information is estimated and attached to the  
105 resulting particle candidate. Since no microscopic simulation is performed and no exact geometry  
106 information is taken into account, the accuracy of this approach is limited, the computation time  
107 on the other hand is orders of magnitude shorter offering the possibility to do studies with higher  
108 statistics.



## 109 4 PID Subsystems

110 The different behavior of charged particles traversing active and passive detector material can be  
111 used to identify (on a probabilistic level) the nature of a charged particle. The PID detectors used  
112 in PANDA take advantage of the following effects:

- 113 • **Specific Energy Loss.** The mean energy loss of charged particles per unit length, usually  
114 referred to as  $dE/dx$ , is described by the Bethe-Bloch equation which depends on the velocity  
115 rather than momentum of the charged particle.
- 116 • **Cherenkov Effect.** Charged particles in a medium with refractive index  $n$  propagating with  
117 velocity  $\beta > 1/n$  emit radiation at an angle  $\Theta_C = \arccos(1/n\beta)$ . Thus, the mass of the  
118 detected particle can be determined by combining the velocity information determined from  
119  $\Theta_C$  with momentum information from the tracking detectors.
- 120 • **Time-of-flight.** Particles with the same momentum, but different masses travel with different  
121 velocities, thus reaching a time-of-flight counter at different times relative to a common start.
- 122 • **Absorption.** A thick layer of passive material absorb most particles due to electromagnetic  
123 ( $e+e-$ ,  $\gamma$ ) or hadronic interactions (all charged and neutral hadrons). After a certain amount  
124 of material only muons and neutrinos survive. The muons can then be detected easily with  
125 any kind of charged particle detector, depending on the desired speed and resolution.

126 The group of subsystems building the particle identification system of PANDA are listed with  
127 growing distance to the Target point:

- 128 • Time Projection Chamber
- 129 • Time of Flight
- 130 • Barrel DIRC
- 131 • Barrel Calorimeter
- 132 • Forward Cherenkov
- 133 • Forward Calorimeter
- 134 • Muon Counter

<sup>135</sup> **4.1 Central Tracker**

figure still missing

Figure 1: GEM-TPC working principle

#### 136 4.1.1 Time Projection Chamber (TPC)

137 The TPC is discussed as a solution for the outer tracking within the target spectrometer (as  
138 Central Tracker). The required momentum resolution is  $\approx 1\%$ , the required vertex resolution  
139  $\approx 150\ \mu\text{m}$  in the xy plane and  $< 1\ \text{cm}$  in z direction.

140 In addition provides the TPC in the momentum range below  $\approx 1\ \text{GeV}/c$  and above  $\approx 2\ \text{GeV}/c$   
141 information for particle identification within the target spectrometer. Especially for particles with  
142 momenta below  $\approx 1\ \text{GeV}/c$  this is of great help for the overall PID performance and to supplement  
143 the information from the barrel DIRC.

144 Working principle

145 General:3D tracking device - charged particles ionize detector gas - electric field along cylinder  
146 axis separates positive gas ions from electrons - primary electrons drift towards readout anode -  
147 gas amplification done by several GEM foils - ungated, continuous operation mode due to HESR  
148 beam properties - intrinsic ion feedback suppression by GEM foils - continuous data readout within  
149 PANDA DAQ - parallel online data reduction and processing (including tracking)

150 PID: performed via measurement of mean energy loss per track length ( $dE/dx$ ), described by  
151 Bethe-Bloch-formula, in combination with (obligatory) momentum measurement - PANDA TPC  
152 offers to do  $\approx 50-100$  (fluctuating) energy loss measurements per track - truncated mean algorithm  
153 used to get rid off Landau tail and to calculate mean.

154 Important values

155 Geometry: inner radius: 15 cm, outer radius: 42cm, length: 150 cm, gas volume: 700l, 2 separate  
156 chambers (due to target pipe)

157 Material budget:  $\frac{X}{X_0} \approx 1.5\%$

158 Detector gas: Ne/CO<sub>2</sub> (90/10, maybe admixture of CH<sub>4</sub>), gas gain: several 1000

159 Operation: drift field: 400 V/cm, 2x2 mm pads (100000)

160 First estimates and simulations (obtained from old PANDA framework and preliminary)

161 Data were generated based on an event generator which shoots p, K, pi, mu and e (plus antipar-  
162 ticles) isotropically through the TPC. All tracks come from the IP, with momenta between 0.2  
163 and 4 GeV/c. Tracks are divided into 6 mm pieces, for each the energy loss is calculated resulting  
164 in 50-100 measurements depending on track length. Upper 40 % are discarded and mean  $dE/dx$   
165 calculated (truncated mean). The spread of the these  $dE/dx$  values for certain p bins is fitted  
166 with a Gaussian and the  $dE/dx$  resolution is defined as the corresponding sigma.

figure still missing

Figure 2: Energy loss in the TPC vs. momentum

figure still missing

Figure 3: Energy loss resolution TPC

167 The separation power between two particles is defined as:

$$\sigma_{sep} = \frac{2 * |I_1 - I_2|}{\left(\frac{\sigma(I_1)}{I_1} + \frac{\sigma(I_2)}{I_2}\right)} \quad (1)$$

168 where I stands for the dE/dx of the respective particle. A constant dE/dx resolution of 5% was  
169 assumed.

170 Note:For all the simulation results shown here the gas density value was a factor of 1.5 to high.  
171 Therefore we expect the performance to be a bit worse. For example the dE/dx resolution will  
172 change from 5% to 7%. Simulations will be repeated with the new PANDA framework as soon  
173 as possible.

figure still missing

Figure 4: TPC separation power vs. momentum

<sup>174</sup> **4.1.2 Straw Tube Tracker (STT)**

175 **4.2 Time of Flight (ToF)**

### 176 4.3 Barrel DIRC

177 The purpose of the Barrel DIRC (Detection of Internal Reflected Cherenkov photons) is to provide  
178 a particle identification. The mass of the particle can be achieved by combining the velocity  
179 information of the DIRC with momentum information from the tracking detectors. In addition  
180 the distinction between gammas and relativistic charged particles entering the EMC behind the  
181 DIRC is possible.

182 Basis for the calculations and simulations are the bar dimensions taken from the BaBar DIRC [3].  
183 With the length adapted to the PANDA setup there are quartz bars of  $17 \times 35 \times 2300 \text{ mm}^3$  and a  
184 distance of 480 mm to the target point. Thus the barrel DIRC covers the solid angle between 22  
185 and 140 degrees. The lower momentum threshold for kaons which produce Cherenkov light is for  
186 an envisaged refractive index of  $n=1.47$  as low as 460 MeV/c for single photon production. For  
187 larger photon numbers the threshold increases.

188 With 17mm (of thickness) of fused silica the DIRC bars present approximately 14% of a radiation  
189 length to normal incident particles. The support structure will add 3%.

190 This design is initially based on the BaBar DIRC [3] but at PANDA further improvements of the  
191 performance are under development. The combination of the spatial image of the photons with  
192 their time of arrival gives access not only to their velocity but also to the wavelength of the photons.  
193 Thus dispersion correction at the lower and upper detection threshold becomes possible. Further  
194 on the reduction of the photon readout in size and number of photon detectors is envisaged. A  
195 lens or a set of lenses at the exit of the quartz bar focus the photons to a focal plane behind a  
196 readout volume of about 30 cm length. When this volume is filled with a medium with the same  
197 refractive index as the radiator material ( $n_{\text{medium}}=n_{\text{radiator}}=1.5$ ) additional dispersion effects and  
198 other image distortions are avoided.

<sup>199</sup> **4.4 Barrel Calorimeter**



## 200 4.5 Forward Cherenkov

201 Two DIRC design options exist for the endcap part of the target spectrometer section. These  
 202 differ in the photon readout design but both use an amorphous fused silica radiator disc. The  
 203 endcap detector position covers forward angles of up to  $\vartheta = 22^\circ$  excluding an inner rectangular (**is**  
 204 **it now elliptical??**) area of  $\vartheta_x = 10^\circ$  horizontal and  $\vartheta_y = 5^\circ$  vertical half-angles. Simulations  
 205 using the DPM generator [4] give  $1.0 \pm 0.8$  (at 2 GeV/c) to  $2.3 \pm 1.8$  (at 15 GeV/c) charged particle  
 206 multiplicity per  $\bar{p}p$  interaction emitted from the target vertex into this acceptance.

207 In such a one-dimensional<sup>1</sup> DIRC type, a photon is transported to the edge of a circular disc while  
 208 preserving the angle information. Avoiding too much light scattering loss at the surface reflections  
 209 requires locally (in the order of millimeters) a surface roughness not exceeding several nanometers  
 210 RMS.

211 The lower velocity threshold, which is common to both designs, depends on the onset of total  
 212 internal reflection for a part of the photons emitted in the Cherenkov cone.

213 There are several boundary conditions for the disc thickness. Radiation length considerations  
 214 as the detector is upstream of the endcap EMC call for a thin disc. The focussing design is  
 215 workable with a 10mm thickness ( $X_0=126\text{mm}$ ). Regarding the mechanical stability and handling  
 216 during polishing, current company feedback recommends 20mm minimum thickness. The resulting  
 217 thickness of the radiator disc has to be a compromise.

---

<sup>1</sup>Light is only reflected on surfaces of one spatial orientation, here the two disc surfaces both normal to the z axis.

### 218 4.5.1 Focussing Disc DIRC

219 In the Focussing Light guide Dispersion-Correcting design (Figures 5 and 6), when a photon  
 220 arrives at the edge of the circular or polygonal disc, it enters into one of about hundred optical  
 221 elements on the rim. Here the two-fold angular ambiguity (up-down) is lifted, the chromatic  
 222 dispersion corrected and the photon focused onto a readout plane. While the optical element  
 223 entered determines the  $\phi$  coordinate, measuring the position in the dispersive direction on the  
 224 focal plane of the focussing light guide yields the  $\theta$  coordinate.

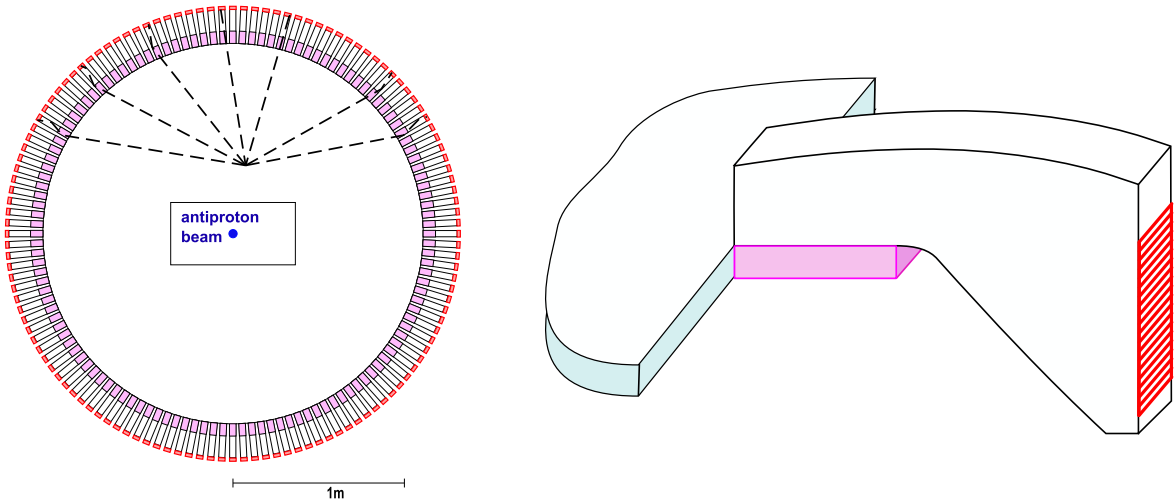


Figure 5: Polyagonal disc with focussing light guides attached to the rim used as optical readout components.

225 Lithium fluoride (LiF) is UV transparent and has particularly low dispersion. Proton beam  
 226 irradiation of a test sample shows that radiation-produced color centers are confined to sufficiently  
 227 small wavelength ranges, and are only partially absorbing at the expected PANDA lifetime dose.  
 228 Hence we believe we can use LiF as a prism element (see Fig. 6) to correct the Cherenkov radiation  
 229 dispersion. The two boundary surfaces, with the radiator disc and the subsequent light guide,  
 230 make the chromatic dispersion correction angle-independent to first order.

231 As with the radiator, the light impinging on the inside of the light guide's curved surface undergoes  
 232 total internal reflection, hence no mirror coating is needed. This reflection makes the focussing  
 233 also independent of the wavelength.

234 With the light staying within the dense optical material of the light guide, most of the incoming  
 235 light phase space from the disc is mapped onto the focal plane with its one-coordinate readout.  
 236 The focussing surface with cylindrical shape of varying curvature has been optimised to give an  
 237 overall minimum for the focus spot sizes of the different angles on the focal plane, individual  
 238 standard deviations being well below 1 mm for the instrumented area.

239 For an Endcap DIRC detector with 128 lightguides and 4096 detector pixels that fits inside the  
 240 target spectrometer return yoke, Figure 8 shows the angle-dependent upper momentum limit being  
 241 about 4–6 GeV/c for  $4\sigma$  pion-kaon separation within the acceptance  $\vartheta=5^\circ-22^\circ$ .

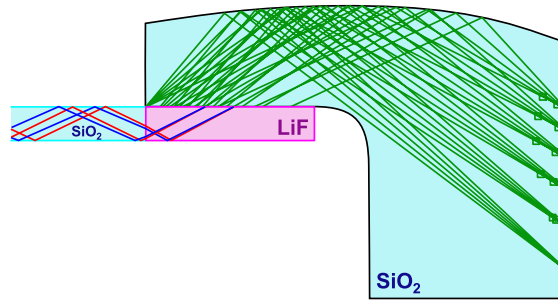


Figure 6: Light guide side view shown with a set of rays used for optimising the light guide curvature. Reflections at the parallel front and back surfaces keep the light inside but do not affect the focussing properties.

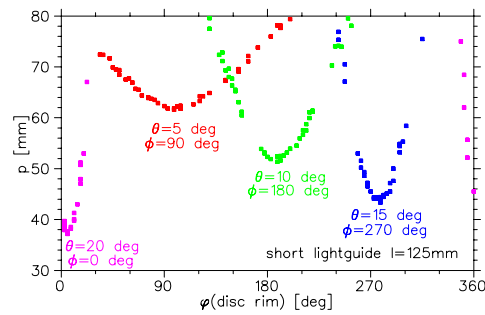


Figure 7: Simulated photon hit pattern for four particles emitted at different angles  $\theta$  and  $\phi$  from the target vertex.

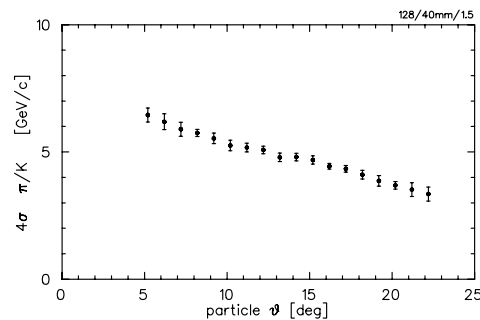


Figure 8: Simulation-derived pion-kaon separation power for a focussing lightguide design with a 15 mm thick amorphous fused silica disc and 0.4 eV photon detection efficiency. Calculation February 2008.

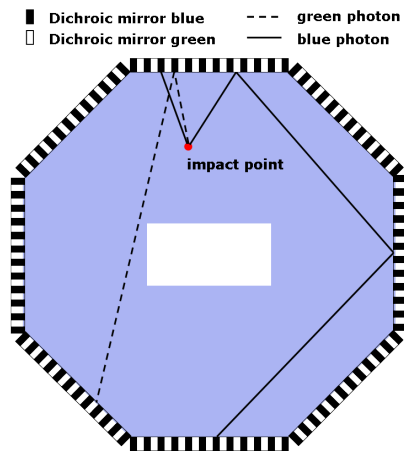


Figure 9: Sketch of the flightpath in the ToP Disc

#### 242 4.5.2 Time of Propagation Disc DIRC

243 In the Multi-Chromatic Time-of-Propagation design ([5]) small detectors measure the arrival time  
 244 of photons on the disc rim, requiring  $\sigma_t=30\text{--}50$  ps single photon time resolution. For any given  
 245 wavelength, the disc edge is effectively covered alternately with mirrors and detectors. Only due to  
 246 the resulting different light path-lengths one can determine accurately enough the start reference  
 247 time, i.e. the time when the initial charged particle enters the radiator, as the stored anti proton  
 248 beam in the HESR has no suitable time structure to be used as an external time start.

249 As some of the light is reflected several times before hitting a detector, the longer path lengths  
 250 allow a better relative time resolution.

251 The use of dichroic mirrors as color filters allows the use of multiple wavelength bands within the  
 252 same radiator (the current design suggesting two bands) resulting in higher photon statistics. The  
 253 narrow wavelength bands minimise the dispersion effects, and the quantum efficiency curve of the  
 254 photo cathode material could be optimised for each wavelength band individually.

255 **4.5.3 Proximity RICH**

256 As alternative approaches Proximity Imaging Solutions were considered.

- 257 • Liquid radiator proximity RICH using CsI GEMs: Proximity focusing RICH detectors use  
258 the most simplest imaging geometry. Their resolution depends on the optical quality and  
259 crucially on the ratio of radiator thickness to stand-off distance, the distance between the cre-  
260 ation and detection of the photon. Using liquid or solid radiators yielding enough Cherenkov  
261 photons, the radiator can be kept rather slim, which in turn only require moderate stand-off  
262 distances on the order of 100 mm. The ALICE HMPID detector is build in this fashion using  
263 a C6F14 liquid radiator and CsI-photon cathodes in an MWPC. This requires a UV optic. It  
264 is proposed to use the same radiator technique and combine the third tracking station with  
265 a CsI coated GEM photon detector. The detector will be thicker along the beam direction  
266 than the DIRC detector previously described, but can be essentially moved to any position  
267 along the beam axis. The estimated performance and the ALICE/STAR test results show  
268 a significant decrease in performance compared to the DIRC solutions.
  
- 269 • Solid radiator proximity RICH using CsI GEMs: One of the main drawbacks of using the  
270 ALICE design is the use of C6F14. This radiator is rather sensitive to impurities and ra-  
271 diation damage requiring a purification system. Using a fused silica disc with a properly  
272 machined surface as radiator circumvents the problem while keeping the geometrical advan-  
273 tages of the design. Initial studies show a further reduction of performance mainly due to  
274 strong dispersive effects in the UV region.
  
- 275 • Aerogel proximity RICH using PMTs: The Belle endcap Cherenkov threshold counter will be  
276 replaced by a proximity imaging RICH counter using an Aerogel radiator and conventional  
277 BiAlkali based multi-pixel PMTs as photon detectors. Using a so-called focusing radiator  
278 scheme, prototypes show excellent performances. The main technological challenge for this  
279 detector is to realise a photon detection matrix in a strong magnetic field. Recent develop-  
280 ments in the field of proximity focusing HAPDs seem to make such a detector realistic. The  
281 large number of pixels required should the detector be placed behind the EMC, but inside  
282 the cryostat merit a detailed look at the costs of such a design.

283 **4.5.4 Forward RICH**

284 **4.6 Forward Calorimeter**

285 **4.7 Muon Counter**



## 286 5 Evaluation

287 Parametrization of the Barrel DIRC: Following the Particle Data Group [[6]] the resolution of the  
288 track Cherenkov angle  $\sigma_{track}$  scales with the square root of the number of photons detected:

$$\sigma_{track}(\Theta) = \frac{\sigma_{single}(\Theta)}{\sqrt{N_{ph}}} \quad (2)$$

289 The  $\Theta$ -dependence comes from the fact that the path length in the detector material varies with  
290 the particle angle which is directly proportional to the number  $N$  of produced Cherenkov photons.

291 Thus we find approximatively the separation of two particle species, i.e. numbers of  $\sigma$  ( $N(\sigma)$ ),  
292 with masses  $m_1$  and  $m_2$ , which pass a radiator of the refraction index  $n$  with the momentum  $p$ :

$$N(\sigma) = \frac{|m_1^2 - m_2^2|}{2p^2\sigma_{track}(\Theta)\sqrt{n^2 - 1}} \quad (3)$$

293 To provide useful results the DIRC should produce 15 to 20 photons per particle track. The  
294 correlation calculated with a photon number of 16 is shown in the figure bellow.

295 A further effect which is very important and specific for DIRC detectors is the capture probability  
296 of the produced light cone from the Cherenkov photons. Depending again on the angle  $\Theta$  of the  
297 incoming particle only a fraction of the photons fulfill the conditions for total internal reflection.  
298 The rest gets lost from the radiator before the first reflection. All known effects are included in  
299 the Fast Simulation (3.3)

### 300 5.1 Potential of the Subsystems

### 301 5.2 Matching of the Subsystems

## 302 6 Global PID Scheme

303 The PANDA spectrometer will feature a complete set of innovative detectors for particle identifi-  
304 cation. The detection of neutral particles will be performed by a highly granular electromagnetic  
305 calorimeter. Charged particles will be identified in the low momentum region by their energy  
306 deposit and ToF, in all other momentum regions by innovative DIRC detectors. The target spec-  
307 trometer will be complemented by a forward spectrometer to detect high momentum particles and  
308 surrounding muon detectors. Each detector systems performance is optimised in itself. Studies  
309 have begun to combine the responses of various detectors in a common framework based on a  
310 likelihood scheme or a carefully trained neural network. These combined likelihood schemes are  
311 successfully employed at various detector systems like HERMEs, Belle and BaBar. They rely on  
312 a reliable parametrisation of the detector component response from simulation and test-beams.  
313 This has to be taken into account in testing PANDA's individual components. The combined  
314 performance of the system will be significantly better than the individual separation powers.

315 **7 Conclusion**

## 316 **8 Acknowledgments**

317 Thanks to analyzers from the "PANDA Physics Book", and all who help with their work and  
318 expertise to the success of the PID TAG.

319 This work is supported by EU FP6 grant, contract number 515873, DIRACsecondary-Beams.

320 **References**

- 321 [1]  $\bar{P}$ ANDA Collaboration, Technical Progress Report, FAI R-ESAC/Pbar 2005
- 322 [2] <http://panda-wiki.gsi.de/cgi-bin/viewauth/Tagpid/WebHome>, Wiki page of the  $\bar{P}$ ANDA  
323 PID TAG
- 324 [3] R. Aleksan et al., Nucl. Inst. Meth. **A397**, 261 (1997)
- 325 [4] A. Galoyan, V.V. Uzhinsky, AIP Conf. Proc. 796, pp. 79-82, 2005
- 326 [5] P. Schönmeier et al., to appear in the proceedings of 6th International Workshop on Ring  
327 Imaging Cherenkov Counters (RICH 2007), Trieste, Italy, 15-20 Oct 2007.
- 328 [6] W.-M. Yao et al. 2006 J. Phys. G: Nucl. Part. Phys. **33** 1

## 329 9 Appendix

### 330 Members of the PID TAG

- 331 • G. Schepers, C. Schwarz - Barrel Dirc (Chairs)
- 332 • B. Kopf, R. Novotny - Barrel Calorimeter
- 333 • B. Seitz - Cherenkov Counter (Global PID)
- 334 • O. Denisov / M. P. Bussa - Muon Counter
- 335 • K. Föhl / P. Vlasov - Forward Cherenkov
- 336 • J. Smyrski / O. Wronska - Forward Calorimeter
- 337 • Q. Weitzel / S. Neubert - Time Projection Chamber
- 338 • C. Schwarz, A. Galoyan - Time of Flight
- 339 • K. Götzen - Fast Simulation
- 340 • K. Peters - Physics